Electronic Supplementary Material (ESI) for Journal of Materials Chemistry C.

Supporting Information

850 nm Pure Near-Infrared Emitting Iridium complex for Solution-processed Organic Light-Emitting Diodes

Yanxin Zhang,[1] Qian Li,[1,2] Minghan Cai,[1] Jie Xue[1,2] and Juan Qiao[1,2] *

Y. Zhang, Dr. Q. Li, M. Cai, Dr. J. Xue and Prof. J. Qiao

Key Lab of Organic Optoelectronics and Molecular Engineering of Ministry of Education

Department of Chemistry

Tsinghua University

Beijing 100084, P. R. China

E-mail: qjuan@mail.tsinghua.edu.cn

Dr. Q. Li, Dr. J. Xue, Prof. J. Qiao

Center for Flexible Electronics Technology

Tsinghua University

Beijing 100084, P. R. China

Table of Contents

Supplementary Experimental Section

1.1. Quantum Chemical Calculation

All of the calculations were carried out with the Gaussian 09 program package using a spin-restricted formalism in the gas phase.[1] The ground and excited electronic states of the complexes were calculated using density functional theory (DFT) and time-dependent DFT (TD-DFT) at the B3LYP level.[2] The standard valence double-ξ polarized basis sets were used for C, H, N, F and S (6-31G*) and Ir (LANL2DZ). An effective core potential (ECP) replaces the inner core electrons of Ir, leaving the outer core [$(5s)^2$ $(5p)^6$] electrons and the $(5d)^6$ valence electrons of Ir(III). The ground state structures of all studied Ir(III) complexes were first optimized with DFT without imposing any symmetry restriction. The optimized structures were then used to calculate the five lowest singlet ($S_0 \rightarrow S_5$) and triplet optical electronic transitions ($S_0 \rightarrow T_5$) using the TD-DFT method. The iridium atom's contributions to the frontier molecular orbits were obtained using the Multiwfn program with Ros-Schuit (SCPA) partition and used to calculate the metal-to-ligand charge transfer (MLCT) percentage in each assignment during the singlet and triplet optical transitions.[3]

1.2. Single-Crystal Structure

The single crystal of **Ir(dotbpa)$_3$** was obtained from diffusion of a chloroform/hexane mixture. The low temperature (104.6K) single-crystals X-ray experiments were performed on a Rigaku RAXIS-SPIDER IP diffractometer with graphite-monochromatized $Mo_{K\alpha}$ radiation (λ=0.71073 Å). Data collection and reduction, cell refinement, and experiential absorption correction for all compounds were performed with the Rigaku RAPID AUTO software package (Rigaku, 1998, Version 2.30). The structure was solved by direct methods and refined against F2 by full-matrix least-squares techniques.

1.3. Photoluminescence measurements

The photoluminescence quantum efficiencies were measured using an absolute photoluminescence quantum yield measurement system (Hamamatsu C9920-02G). Absorption spectra were recorded using a UV-vis spectrophotometer (Agilent 8453). The emission spectra and the transient photoluminescence measurements were carried out using a transient spectrometer (Edinburg FL920P). The time-resolved PL spectra were measured on a laser flash photolysis spectrometer (Edingburg LP-920). The 1×10^{-5} M solution was used for photoluminescence spectra measurement. And films for optical measurements were fabricated by drop-coating onto clean quartz substrates.

1.4. Fabrication and Characterization of OLEDs

Before device fabrication, the prepatterned indium tin oxide (ITO) glass substrates were carefully cleaned and treated by an UV-ozone for 6 min. Then 40-50 nm poly (3,4-ethylenedioxythiophene) (PEDOT: PSS, Bayer Baytron P8000) used as a hole injection layer was spin-coated on the ITO substrate and baked at 200 ^{o}C for 10 min in a nitrogen glovebox. The emitting layer was spin-coated onto the PEDOT: PSS-coated substrate from 1,2-dichloroethane solutions and then annealed at 80 ^{o}C for 30 min to remove the solvent residue. Afterwards, the substrates were transferred into an evaporation chamber integrated with the glovebox for the deposition of

electron-transporting layer and metal cathode. 4,7-diphenyl-1,10-phenanthroline (Bphen) was evaporated as the electron-transporting layer at a rate of 0.5-1 Å/s under a pressure of 4×10^{-4} Pa. Finally, the LiF/Al bilayer cathode was evaporated at rates of 0.1 Å/s and 5-10 Å/s, respectively, under a base pressure of 4×10^{-4} Pa. The current density-voltage characteristics were measured with a Keithley 4200 semiconductor characterization system, and optical power was recorded on a Newport 1936-C power meter coupled to a calibrated Newport 918D-UV-OD3 detector with a spectral response range from 200 to 1100 nm. Electrophosphorescent spectra were collected with a Jobin Yvon FluoroMax-3 fluorospectrophotometer. All measurements were carried out in air at room temperature with encapsulation.

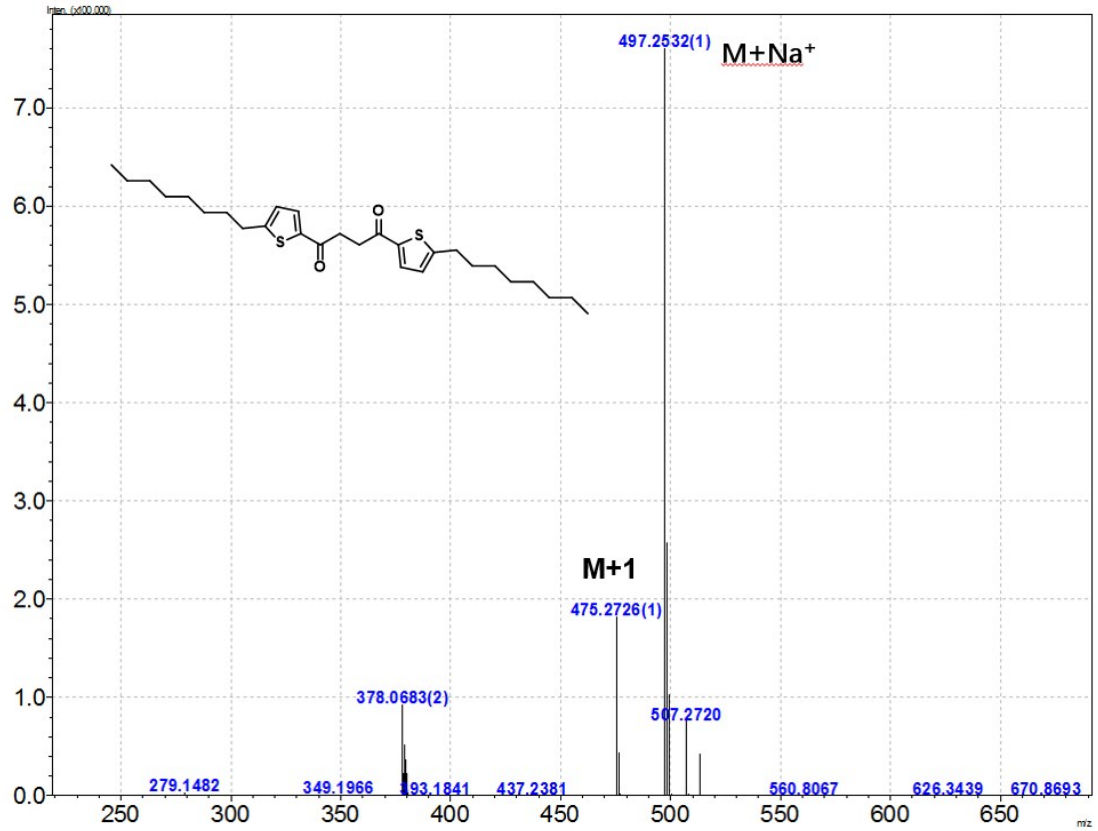

Figure S1. HRMS-ESI+ spectrum of 1,4-bis(5-octyl-2-thienyl)-1,4-Butanedione (**1**)

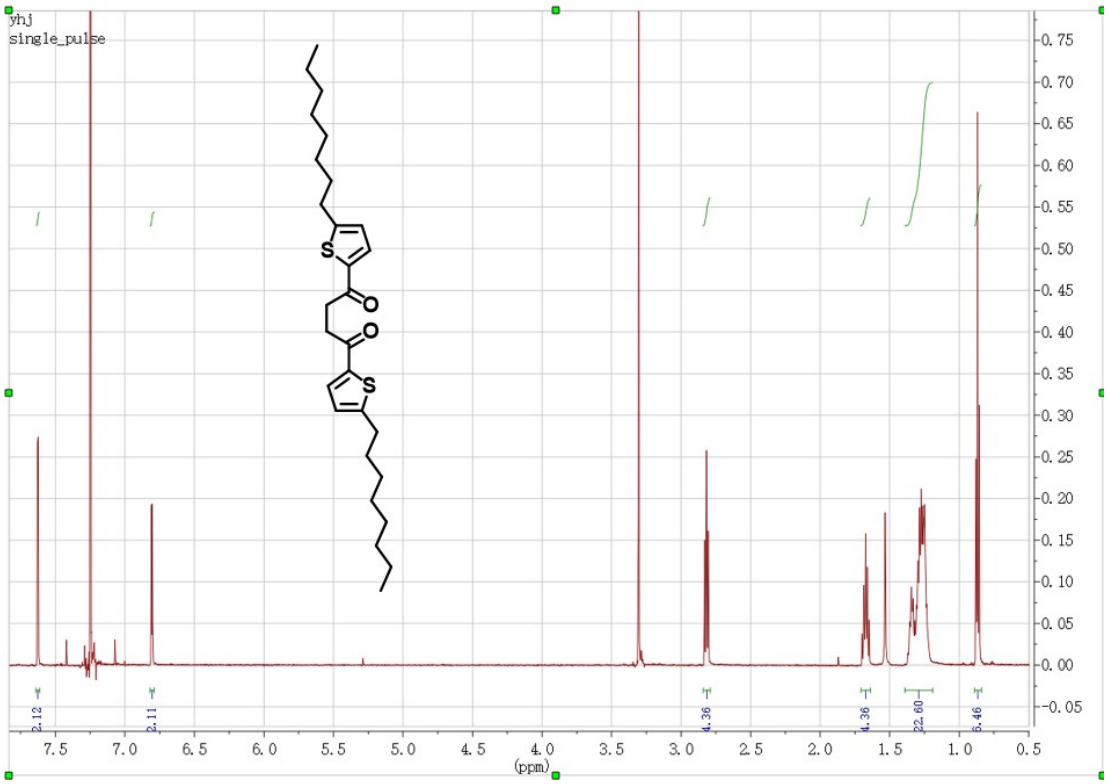

Figure S2. ^{1}H NMR spectrum of 1,4-bis(5-octyl-2-thienyl)-1,4-Butanedione (**1**)

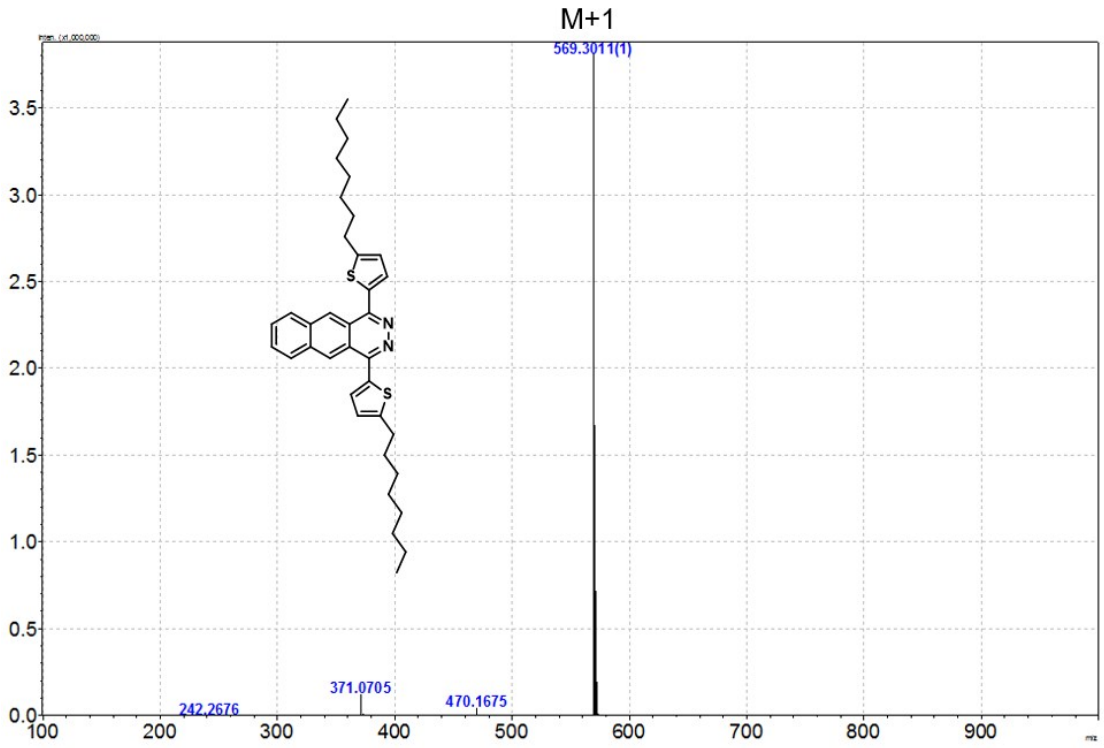

Figure S3. HRMS-ESI$^+$ spectrum of 1,4-di(5-octyl-thiophen-2-yl)benzo[g]phthalazine (**dotbpaH**)

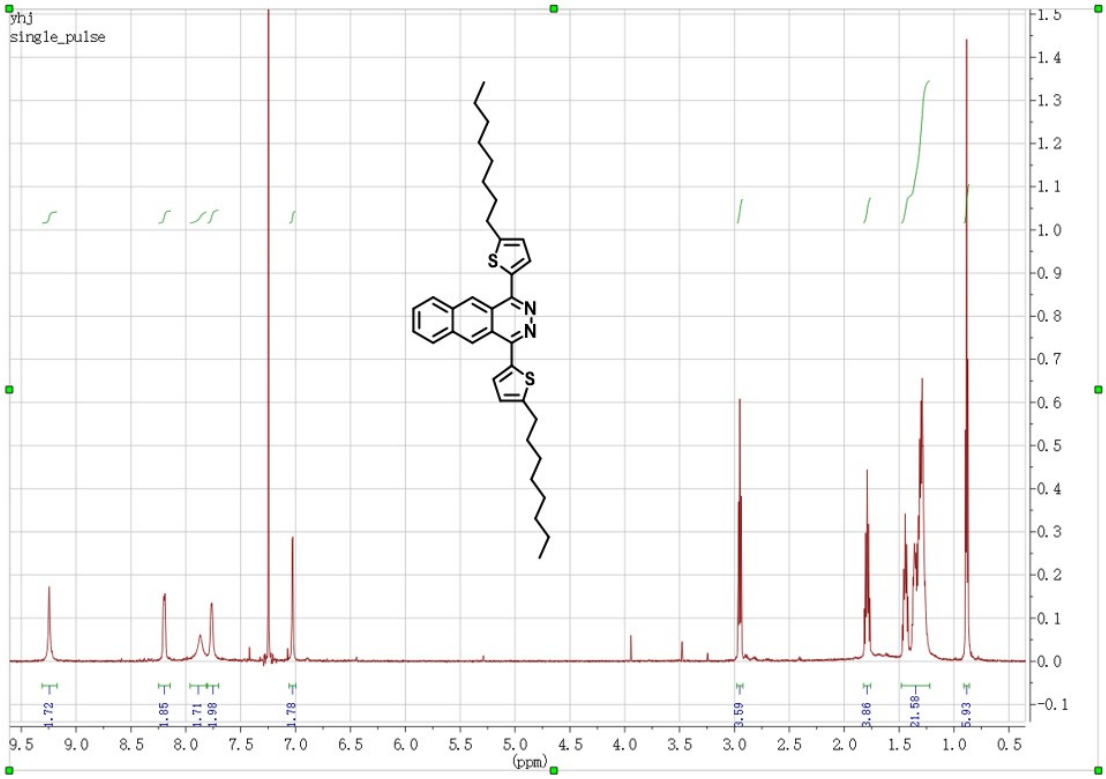

Figure S4. ^{1}H NMR spectrum of 1,4-di(5-octyl-thiophen-2-yl)benzo[g]phthalazine (**dotbpaH**)

Figure S5. Photo of 1,4-bis(5-octyl-2-thienyl)-1,4-Butanedione (**1**) (left) and 1,4-di(5-octyl-thiophen-2-yl)benzo[g]phthalazine (**dotbpaH**) (right)

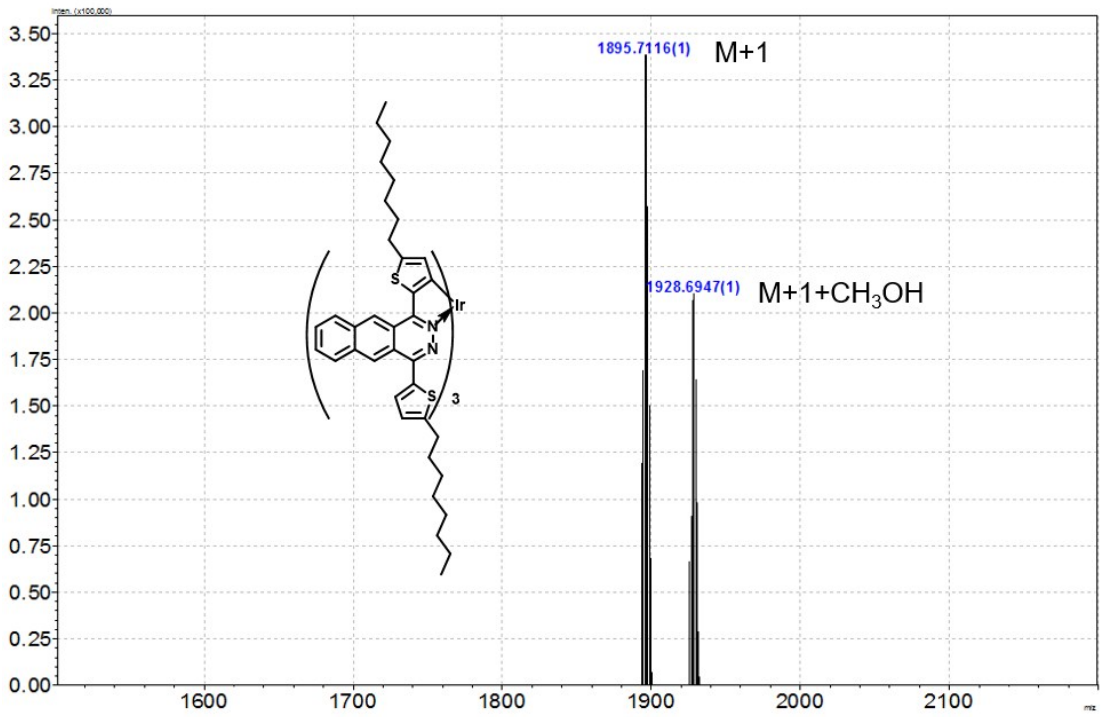

Figure S6. HRMS-ESI$^+$ spectrum of tris[1,4-di(5-n-octylthiophen-2-yl)benzo[g]phthalazine] iridium(III) (**Ir(dotbpa)$_3$**)

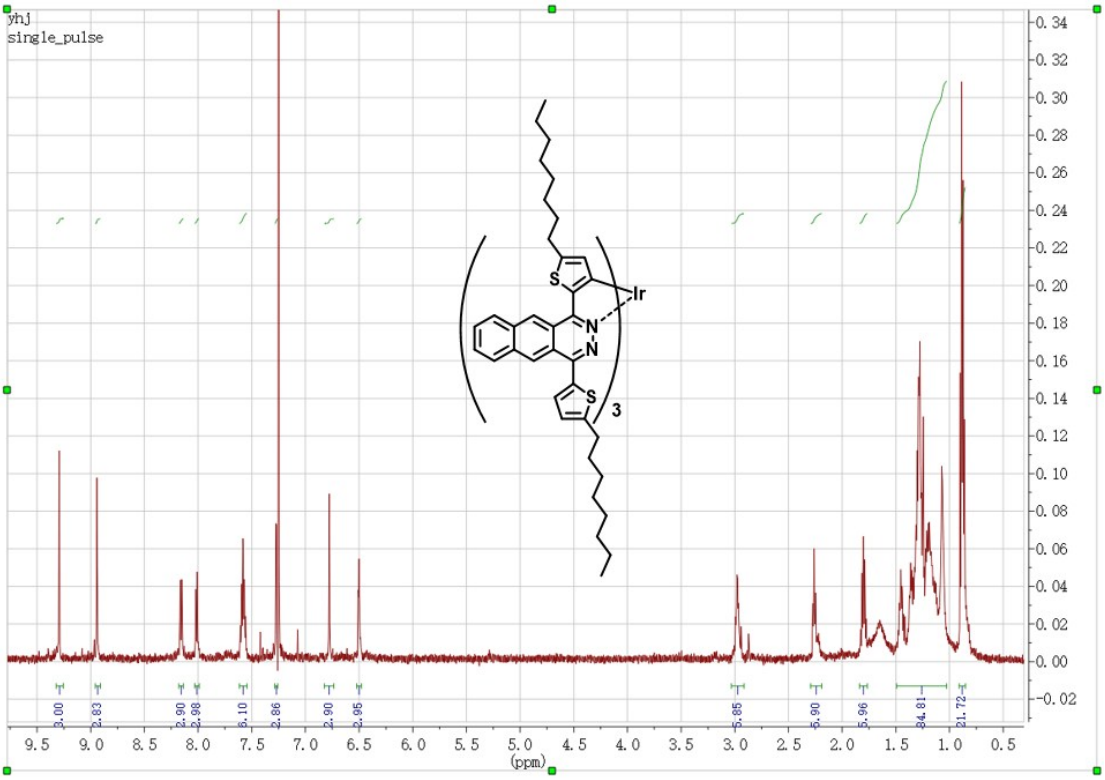

Figure S7. ^{1}H NMR spectrum of tris[1,4-di(5-n-octylthiophen-2-yl)benzo[g]phthalazine] iridium(III) (**Ir(dotbpa)$_3$**)

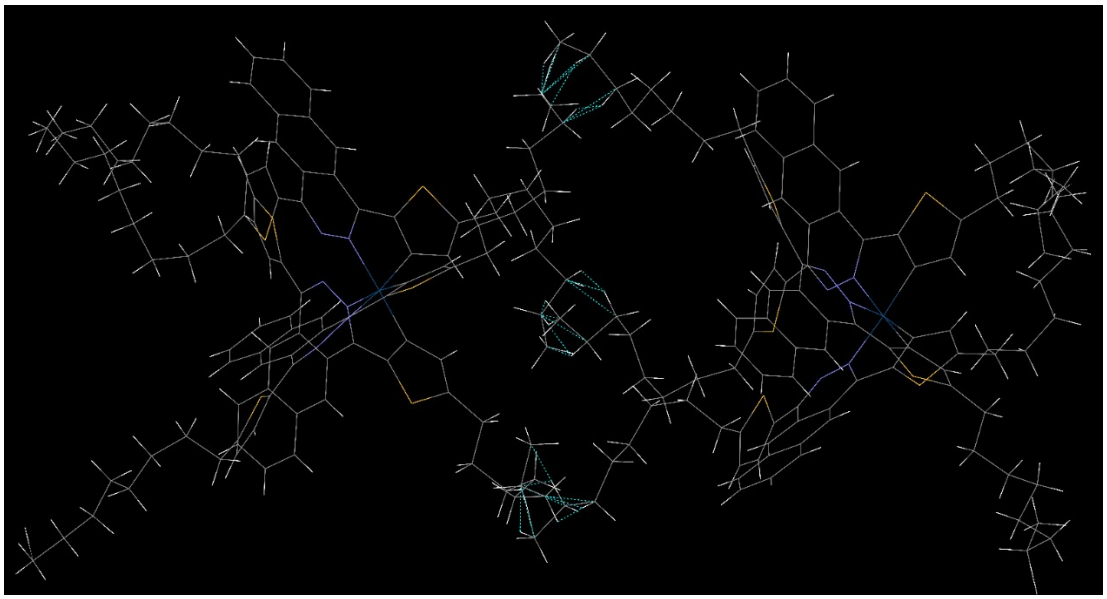

Figure S8. Intermolecular interactions between neighbouring molecules in the single-crystal of **Ir(dotbpa)$_3$**.

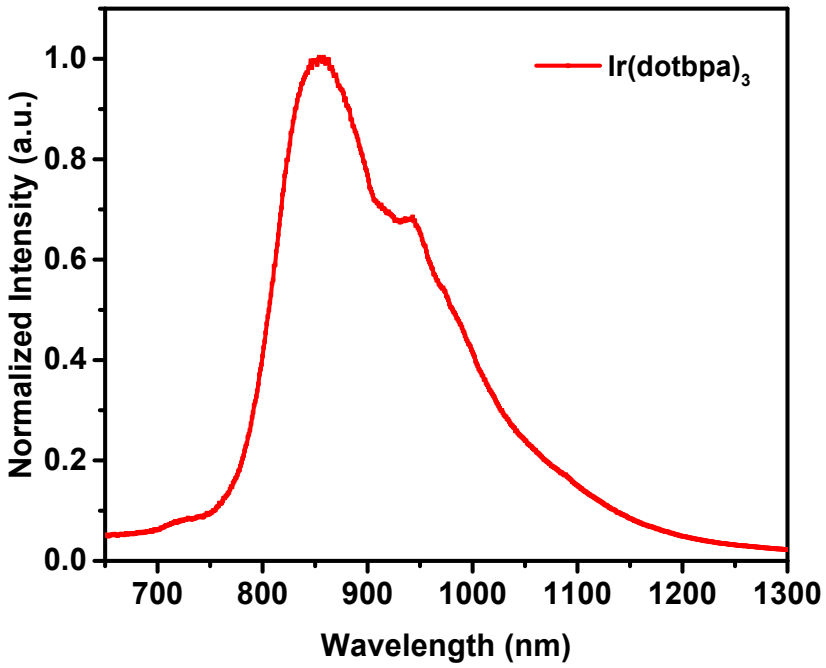

Figure S9. PL emission spectrum of **Ir(dotbpa)$_3$** doped in PMMA film (5 wt%)

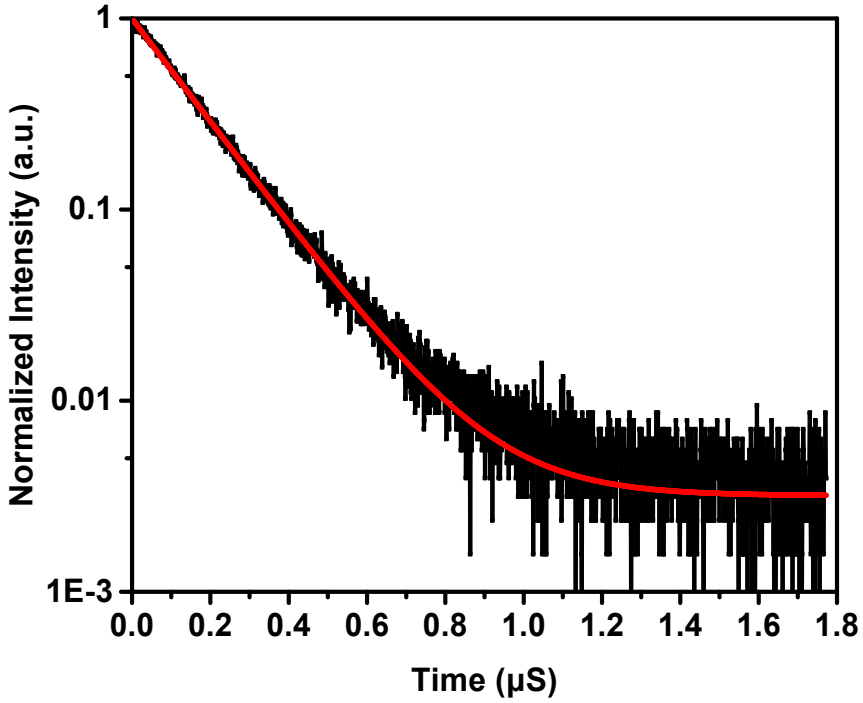

Figure S10. Transient phosphorescence decay of **Ir(dotbpa)$_3$** in CH_2Cl_2 at 298 K. Red curves are exponential fitting data.

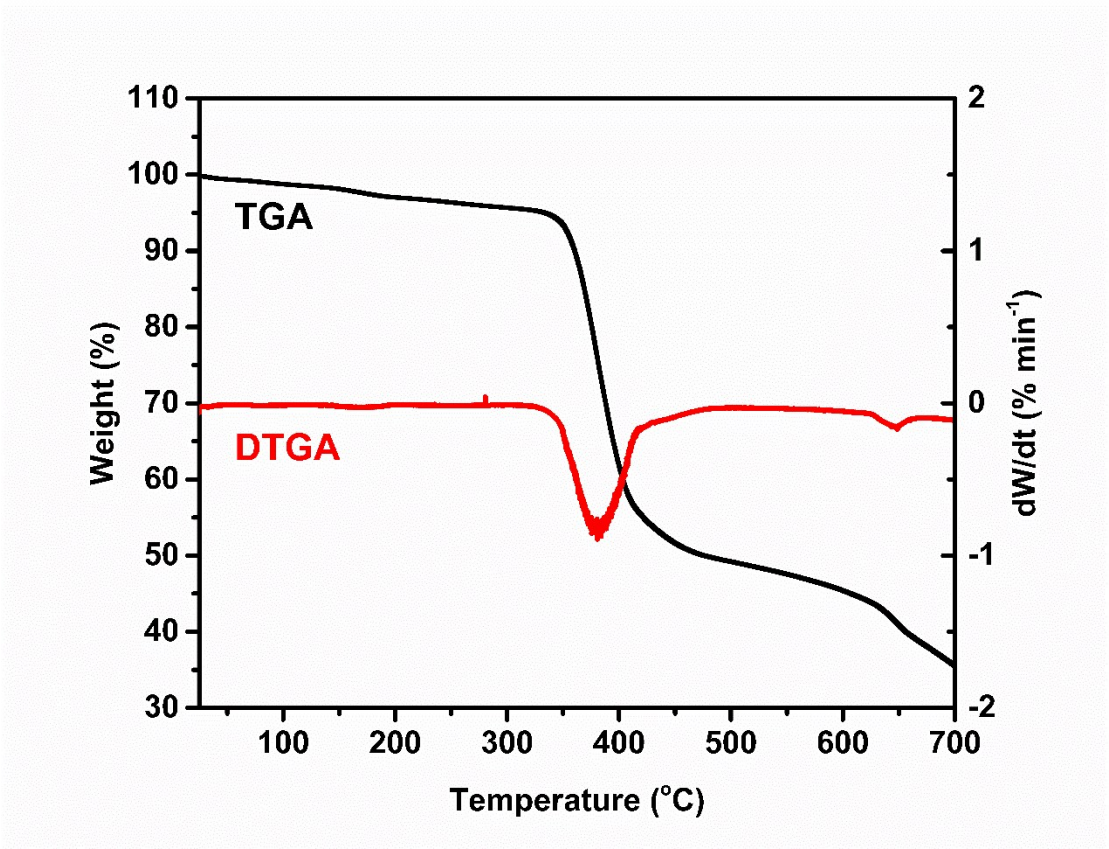

Figure S11. TGA and DTGA curve of **Ir(dotbpa)$_3$** in N_2 with heating rate of 10 °C min^{-1}.

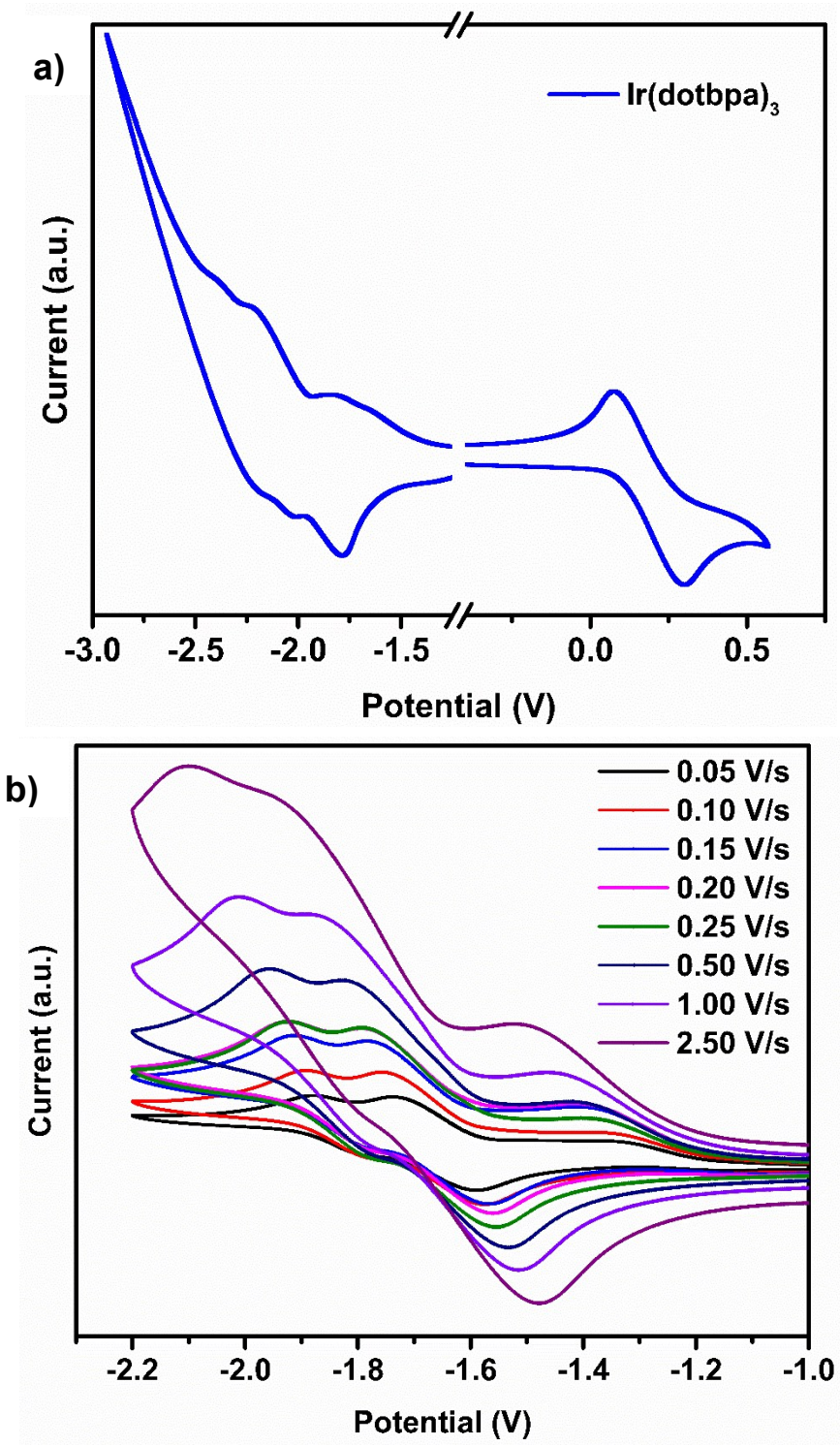

Figure S12. a) Cyclic voltammograms of **Ir(dotbpa)$_3$** recorded versus Fc^+/Fc in anhydrous THF solutions at 298 K under N_2 atmosphere (scan rate = 150 mV s^{-1}); b) Reduction scans of **Ir(dotbpa)$_3$** recorded under different scan rates in anhydrous THF solutions at 298 K under N_2 atmosphere.

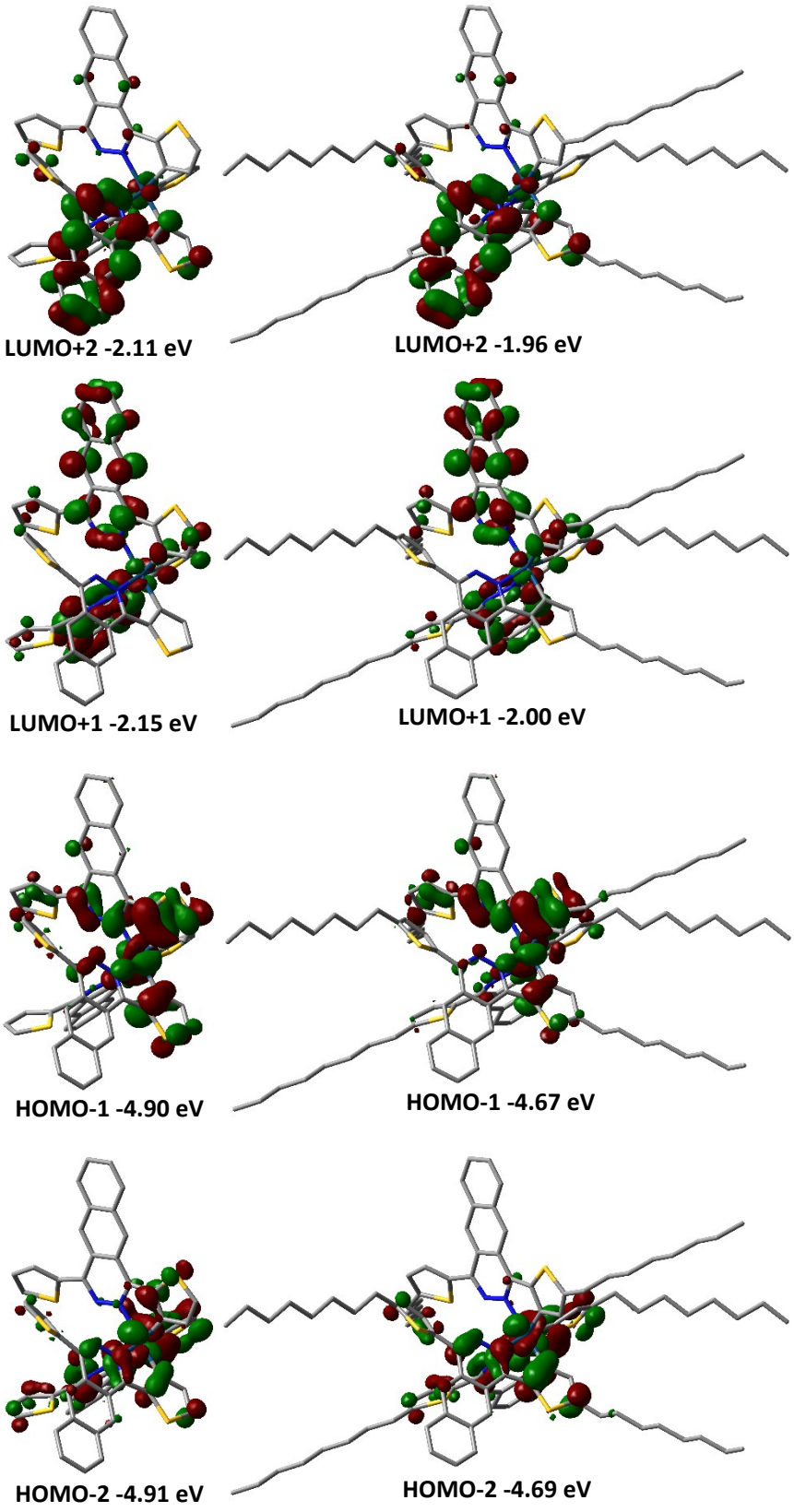

Figure S13. Frontier orbitals and molecular surfaces of $Ir(dtbpa)_3$ and **$Ir(dotbpa)_3$**. All the MO surfaces correspond to an isocontour value of $|\Psi| = 0.03$. Hydrogen atoms were hidden for better view.

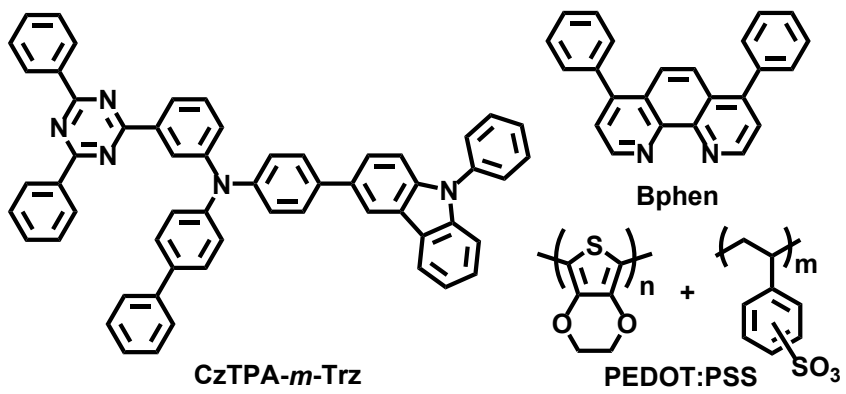

Figure S14. Molecular structures used in NIR-OLED devices.

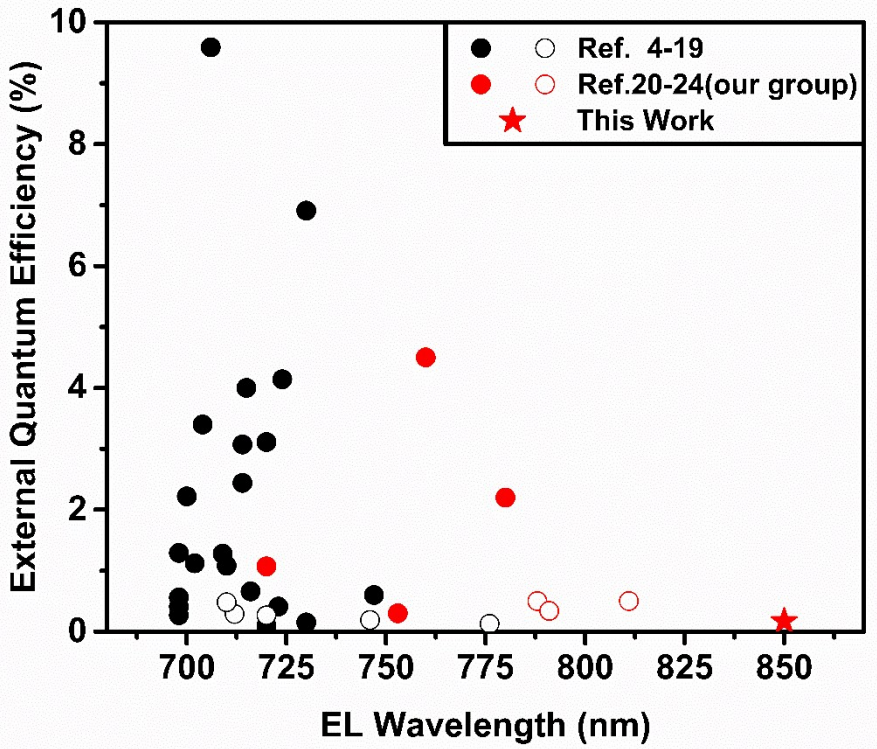

Figure S15. EQEs versus EL peaks for reported NIR-OLEDs based on Ir(III) emitters. Solid symbols: energy fully transferred from hosts to Ir(III) emitters; Open symbols: incomplete energy transfer. Black dots: Ref. 4-19; Red dots: Ref. 20-24(our group's works); Red Star: this work.

Table S1. Summary of characteristics of NIR-OLEDs fabricated with Ir complexes reported so far.

Emitter Name in Ref.	PLQY (%)[a)]	Device Structure	λ_{EL} (nm)[b)]	EQE (%)	Radiance ($mW \cdot cm^{-2}$)	Ref.
NIR1		ITO/PEDOT/PVK:PBD:NIR1(5%)/LiF/Al	720	0.097	0.119	4
NIR1		ITO/PEDOT/PVK:PBD:NIR1(5%)/BCP/Alq_3/LiF/Al	720	0.266	0.238	4
Ir-3	0.057	ITO/PEDOT:PSS/CBP:Ir-3(2%)/BCP/Alq_3/LiF/Al	533, 746, 825sh	0.189		5
Ir-4	too weak	ITO/PEDOT:PSS/CBP:Ir-4(2%)/BCP/Alq_3/LiF/Al	538, 776, 836sh	0.127		5
$(thdpqx)_2Ir(acac)$	14.9	ITO/PEDOT/PVK: 40 wt%PBD:$(thdpqx)_2$Ir-(acac)(1%)/TPBi/CsF/Al	704	3.4	0.444	6
$(CH3OTPA\text{-}BTz\text{-}Iq)_2Irpic$		ITO/PEDOT:PSS/PVK:OXD-7(70:30):(CH_3OTPA-BTzIq)$_2$Irpic(12%)/TPBI/Ba/Al	723, 780(sh)	0.41	0.0741	7
1	16	ITO/PEDOT:PSS/PVK(65%):OXD7(30%):1(5%)/Ba/Al	714	3.07	1.43 $Wsr^{-1}m^{-2}$	8
2	7	ITO/PEDOT:PSS/PVK(65%):OXD7(30%):2(5%)/Ba/Al	709	1.28	3.1 $Wsr^{-1}m^{-2}$	8
3	14	ITO/PEDOT:PSS/PVK(65%):OXD7(30%):3(5%)/Ba/Al	714	2.44	4.9 $Wsr^{-1}m^{-2}$	8
$(t\text{-}BuPyrPyTPA)_2Ir$ (acac)	1.92	ITO/PEDOT/PVK:30 wt% OXD-7:(t-BuPyrPyTPA)$_2$Ir(acac)(4%)/TPBi/Ba/Al	698, 763	0.56	0.0543	9
Mono-Ir	2.25	ITO/PEDOT:PSS/TFB/CBP:PBD:Mono-Ir(60:30:10)/TmPyPB/Liq/Al	698, 762	1.29	0.59 $mWsr^{-1}cm^{-2}$	10
D-Ir-Caz	0.7	ITO/PEDOT:PSS/TFB/CBP:PBD:D-Ir-Caz(60:30:10)/TmPyPB/Liq/Al	698, 762	0.27	0.54 $mWsr^{-1}cm^{-2}$	10
D-Ir-OXD	1.22	ITO/PEDOT:PSS/TFB/CBP:PBD:D-Ir-OXD(60:30:10)/TmPyPB/Liq/Al	698, 762	0.41	0.62 $mWsr^{-1}cm^{-2}$	10
1	13	ITO/PEDOT:PSS/PVK:OXD7:1(5%)/TmPyPB/LiF/Al	700, 760(sh)	2.22	0.11 $Wsr^{-1}m^{-2}$	11
Ir3	1.1	ITO/PEDOT:PSS/mCP:TCTA:Ir3/TPBi/Liq/Al	747	0.6		12
Ir4	10.6	ITO/PEDOT:PSS/mCP:TCTA:Ir4/TPBi/Liq/Al	730	0.15		12
Ir6	1.8	ITO/HAT-CN/TAPC/mCP:Ir6(10%)/TmPyPB/LiF/Al	715	4		13
1	8	ITO/PEDOT:PSS/PVK:OXD7:1(5%)/TmPyPB/LiF/Al	702, 772(sh)	1.12	0.047 $W/sr \cdot m^2$	14
2	15	ITO/PEDOT:PSS/PVK:OXD7:2(5%)/TmPyPB/LiF/Al	720	3.11	0.140 $W/sr \cdot m^2$	14
$(TPA\text{-}BTz\text{-}Iq)_2pic$	0.2	ITO/PEDOT:PSS/PVK/CBP:(TPA-BTz-Iq)$_2$pic(9%)/TPBI/Ba/Al	712	0.29	0.079	15
$(tBuTPA\text{-}BTz\text{-}Iq)_2pic$	0.5	ITO/PEDOT:PSS/PVK/CBP:(tBuTPA-BTz-Iq)$_2$pic(9%)/TPBI/Ba/Al	716	0.66	0.123	15
$(FTPA\text{-}BTz\text{-}Iq)_2Irpic$	0.3	ITO/PEDOT:PSS/PVK/CBP:(FTPA-BTz-Iq)2Irpic(12%)/TPBI/Ba/Al	710	0.48	0.085	15
$(PPz\text{-}11,12\text{-}DO)_2Ir(acac)$	13	ITO/PEDOT:PSS/poly-TPD/PVK:OXD-7(7:3): /TmPyPB/LiF/ Al	724	4.14	20.981 $Wsr^{-1}m^{-2}$	16
1	1	ITO/PEDOT:PSS/PVK:OXD-7:1/LiF/Al	710	1.08	14.9 $W/sr \cdot cm^2$	17
TCNIr	6	ITO/HATCN/TAPC/mCP/TCNIr in CBP (15 wt%)/TPBi/LiF/Al	706	9.59		18
Ir-R	0.28	ITO/PEDOT: PSS/poly-TPD/CBP:Ir-R(1%)/TmPyPB/CsF/Al	730	6.91	26.1 W Sr^{-1} m^{-2}	19
$Ir(pbq\text{-}g)_2acac$	2.5	ITO/NPB/Alq_3:Ir(pbq-g)$_2$acac(10%)/Alq3/Mg:Ag	720, 780(sh)	1.07	4.6	20
2	0.2	ITO/PEDOT:PSS/PVK:30 wt%PBD or OXD-7: 2(20%)/TPBI/Cs2CO3/Al	753	0.3	0.095	21
1	1.5	ITO/NPB/$Ga_2(saph)_2q_2$:1(20%)/Bphen/Mg:Ag	780, 850(sh)	2.2	1.8	22
1	3.1	ITO/PEDOT:PSS/PVK:30 wt% PBD:1(20 wt%)/TPBI/Cs_2CO_3/Al	715(sh), 788	0.5	0.1112	23
2	2.9	ITO/PEDOT:PSS/PVK:30 wt% PBD:2(20 wt%)/TPBI/Cs_2CO_3/Al	791	0.34	0.0572	23
1	2.9	ITO/NPB/DIC-TRZ:1(6%)/TPBi/Mg:Ag	811	0.5	0.0945	24
2	14.7	ITO/NPB/DIC-TRZ:2(12%)/TPBi/Mg:Ag	760	4.5	4.1818	24

a) measured in solution. b) sh represent shoulder peak.

Table S3. Average bond lengths and angles of $Ir(dtbpa)_3$ and **$Ir(dotbpa)_3$** from quantum chemical calculations and X-ray crystallography data.

	Ir-C bond lengths (Å)	Ir-N bond lengths (Å)	C-Ir-N Angles (º)
$Ir(dtbpa)_{3\ Crystal}$	2.014	2.098	78.26
$Ir(dtbpa)_{3\ Calculation}$	2.008	2.159	77.69
$Ir(dotbpa)_{3\ Crystal}$	2.013	2.089	78.80
$Ir(dotbpa)_{3\ Calculation}$	2.008	2.162	77.72

Table S4. Selected excited states for $Ir(dtbpa)_3$ and **$Ir(dotbpa)_3$** calculated from TDDFT approach.

Complex	States (E[eV]) (λ[nm])[a]	Dominant excitations[b]	Character	Assignment	MLCT (%)
$Ir(dtbpa)_3$	T_1 (1.494) (830)	H → L (57%) H-1 → L+1 (15%) H-2 → L+1 (13%)	π(dtbpa)/dπ(Ir) → π*(dtbpa) π(dtbpa)/dπ(Ir) → π*(dtbpa) π(dtbpa)/dπ(Ir) → π*(dtbpa)	MLCT/ILCT/LLCT	29.69
	T_2 (1.5099) (821)	H → L+1 (44%) H-1→L (21%) H-2→L (13%)	π(dtbpa)/dπ(Ir) → π*(dtbpa) π(dtbpa)/dπ(Ir) → π*(dtbpa) π(dtbpa)/dπ(Ir) → π*(dtbpa)	MLCT/ILCT/LLCT	27.96
	T_3 (1.534) (808)	H→L+2 (43%) H-2→L+2 (13%) H-1→L+2 (11%) H-2→L (11%)	π(dtbpa)/dπ(Ir) → π*(dtbpa) π(dtbpa)/dπ(Ir) → π*(dtbpa) π(dtbpa)/dπ(Ir) → π*(dtbpa) π(dtbpa)/dπ(Ir) → π*(dtbpa)	MLCT/ILCT/LLCT	27.97
	S_1 (1.9617) (632)	H→L (100%)	π(dtbpa)/dπ(Ir) → π*(dtbpa)	MLCT/ILCT	34.82
$Ir(dotbpa)_3$	T_1 (1.441) (860)	H → L (52%) H-1 → L+1 (21%) H-2 → L (9%)	π(dotbpa)/dπ(Ir) → π*(dotbpa) π(dotbpa)/dπ(Ir) → π*(dotbpa) π(dotbpa)/dπ(Ir) → π*(dotbpa)	MLCT/ILCT/LLCT	24.88
	T_2 (1.4552) (852)	H → L+1 (45%) H-1→L (30%) H-1 → L+1 (10%)	π(dotbpa)/dπ(Ir) → π*(dotbpa) π(dotbpa)/dπ(Ir) → π*(dotbpa) π(dotbpa)/dπ(Ir) → π*(dotbpa)	MLCT/ILCT/LLCT	23.32
	T_3 (1.4954) (829)	H→L+2 (39%) H-2→L+2 (26%) H-2→L (16%)	π(dotbpa)/dπ(Ir) → π*(dotbpa) π(dotbpa)/dπ(Ir) → π*(dotbpa) π(dotbpa)/dπ(Ir) → π*(dotbpa)	MLCT/ILCT/LLCT	23.36
	S_1 (1.9222) (645)	H→L (100%)	π(dotbpa)/dπ(Ir) → π*(dotbpa)	MLCT/ILCT	30.42

[a] Data in parentheses are excitation energies and corresponding wavelengths. [b] H and L denote HOMO and LUMO, respectively; data

in parentheses are the contributions of corresponding excitations.

Table S5. Contribution of iridium and n-octyl groups to selected HOMOs of $Ir(dtbpa)_3$ and **$Ir(dotbpa)_3$**.

	Contribution of iridium (%)		Contribution of n-octyl groups (%)
Molecular orbital	$Ir(dtbpa)_3$	$Ir(dotbpa)_3$	$Ir(dotbpa)_3$
HOMO	35.16	30.74	3.20
HOMO-1	23.90	18.36	3.99
HOMO-2	23.84	18.61	3.89

References

1 Gaussian 09, Revision A.02, M. J. Frisch, G. W. Trucks, H. B. Schlegel, G. E. Scuseria, M. A. Robb, J. R. Cheeseman, G. Scalmani, V. Barone, G. A. Petersson, H. Nakatsuji, X. Li, M. Caricato, A. Marenich, J. Bloino, B. G. Janesko, R. Gomperts, B. Mennucci, H. P. Hratchian, J. V. Ortiz, A. F. Izmaylov, J. L. Sonnenberg, D. Williams-Young, F. Ding, F. Lipparini, F. Egidi, J. Goings, B. Peng, A. Petrone, T. Henderson, D. Ranasinghe, V. G. Zakrzewski, J. Gao, N. Rega, G. Zheng, W. Liang, M. Hada, M. Ehara, K. Toyota, R. Fukuda, J. Hasegawa, M. Ishida, T. Nakajima, Y. Honda, O. Kitao, H. Nakai, T. Vreven, K. Throssell, J. A. Montgomery, Jr., J. E. Peralta, F. Ogliaro, M. Bearpark, J. J. Heyd, E. Brothers, K. N. Kudin, V. N. Staroverov, T. Keith, R. Kobayashi, J. Normand, K. Raghavachari, A. Rendell, J. C. Burant, S. S. Iyengar, J. Tomasi, M. Cossi, J. M. Millam, M. Klene, C. Adamo, R. Cammi, J. W. Ochterski, R. L. Martin, K. Morokuma, O. Farkas, J. B. Foresman, and D. J. Fox, Gaussian, Inc., Wallingford CT, 2016.

2 a) C. Lee, W. Yang, R. G. Parr, *Phys. Rev. B* 1988, **37**, 785; b) A. D. Becke, *J. Chem. Phys.* 1993, **98**, 5648.

3 a) T. Lu, F. Chen, *J. Comput. Chem.* 2012, **33**, 580; b) P. Ros, G. C. A. Schuit, *Theoretica chimica acta* 1966, **4**, 1.

4. E. L. Williams, J. Li and G. E. Jabbour, *Appl. Phys. Lett.*, 2006, **89**, 083506.

5. C.-L. Ho, B. Yao, B. Zhang, K.-L. Wong, W.-Y. Wong, Z. Xie, L. Wang and Z. Lin, *Journal of Organometallic Chemistry*, 2013, **730**, 144–155.

6. X. Cao, J. Miao, M. Zhu, C. Zhong, C. Yang, H. Wu, J. Qin and Y. Cao, *Chem. Mater.*, 2015, **27**, 96–104.

7. J. Yu, H. Tan, F. Meng, K. Lv, W. Zhu and S. Su, *Dyes and Pigments*, 2016, **131**, 231–238.

8. S. Kesarkar, W. Mróz, M. Penconi, M. Pasini, S. Destri, M. Cazzaniga, D. Ceresoli, P. R. Mussini, C. Baldoli, U. Giovanella and A. Bossi, Angew. *Chem. Int. Ed.*, 2016, **55**, 2714–2718.

9. Y. Liu, Z. Hao, F. Meng, P. Wang, L. Yang, Y. Wang, Y. Pei and S. Su, *Chemical Physics Letters*, 2018, **699**, 99–106.

10. Z. Hao, M. Li, Y. Liu, Y. Wang, G. Xie and Y. Liu, *Dyes and Pigments*, 2018, **149**, 315–322.

11. G. Fu, H. Zheng, Y. He, W. Li, X. Lü and H. He, *J. Mater. Chem. C*, 2018, **6**, 10589–10596.

12. H. U. Kim, S. Sohn, W. Choi, M. Kim, S. U. Ryu, T. Park, S. Jung and K. S. Bejoymohandas, *J. Mater. Chem. C*, 2018, **6**, 10640–10658.

13. Z. Chen, L. Wang, C.-L. Ho, S. Chen, S. Suramitr, A. Plucksacholatarn, N. Zhu, S. Hannongbua and W.-Y. Wong, *Advanced Optical Materials*, 2018, **6**, 1800824.

14. J. Zhou, G. Fu, Y. He, L. Ma, W. Li, W. Feng and X. Lü, *Journal of Luminescence*, 2019, **209**, 427–434.
15. J. Yu, C. Xu, F. Meng, H. Tan, M. Li and W. Zhu, *Dyes and Pigments*, 2019, **166**, 307–313.
16. C. You, D. Liu, F. Meng, Y. Wang, J. Yu, S. Wang, S. Su and W. Zhu, *J. Mater. Chem. C*, 2019, **7**, 10961–10971.
17. Y. He, G. Fu, W. Li, B. Wang, T. Miao, M. Tan, W. Feng and X. Lü, *Journal of Luminescence*, 2020, **218**, 116847.
18. Z. Chen, H. Zhang, D. Wen, W. Wu, Q. Zeng, S. Chen and W.-Y. Wong, *Chem. Sci.*, 2020, **11**, 2342–2349.
19. C. You, D. Liu, M. Zhu, J. Yu, B. Zhang, Y. Liu, Y. Wang and W. Zhu, *J. Mater. Chem. C*, 2020, DOI:10.1039/D0TC00479K.
20. J. Qiao, L. Duan, L. Tang, L. He, L. Wang and Y. Qiu, *J. Mater. Chem.*, 2009, **19**, 6573–6580.
21. R. Tao, J. Qiao, G. Zhang, L. Duan, L. Wang and Y. Qiu, *J. Phys. Chem. C*, 2012, **116**, 11658–11664.
22. R. Tao, J. Qiao, G. Zhang, L. Duan, C. Chen, L. Wang and Y. Qiu, *J. Mater. Chem. C*, 2013, **1**, 6446–6454.
23. L. Xin, J. Xue, G. Lei and J. Qiao, *RSC Adv.*, 2015, **5**, 42354–42361.
24. J. Xue, L. Xin, J. Hou, L. Duan, R. Wang, Y. Wei and J. Qiao, *Chem. Mater.*, 2017, **29**, 4775–4782.